ACS Catalysis

pubs.acs.org/acscatalysis Research Article

Controlling Cubic versus Octahedral Morphology in Plasmonic Aluminum Nanoparticle Synthesis with Titanocene Catalysts: A Systematic Study

Jaekwan Kim, Christian R. Jacobson, Naomi J. Halas, and Ian A. Tonks*

Cite This: ACS Catal. 2024, 14, 18429−18435 Read Online

ACCESS | Metrics & More | Article Recommendations | Supporting Information

ABSTRACT: Ti precatalysts containing the titanocene moiety (Cp_2Ti−, Cp = cyclopentadienyl) can, under certain conditions, selectively produce cubic Al nanocrystals through the dehydrocoupling of alane amine adducts such as $AlH_3{\cdot}NMe_2Et$. A systematic study of reaction conditions reveals that cubic Al nanoparticle formation occurs at a higher temperature (e.g., 65 °C) and/or higher catalyst-concentration conditions (e.g., 0.5 mol % [Ti]). Kinetic studies reveal that under these conditions nanoparticle formation and alane consumption are much faster, and cubic nanoparticle formation takes place under kinetically controlled conditions. On the other hand, employing a wide suite of TiX_4 (X = anionic ligand)-type precatalysts yielded only octahedral-shaped aluminum nanoparticles regardless of conditions. Finally, we report the synthesis of a hydride-bridged Ti−Al heterobimetallic compound from the reaction of Cp_2TiCl_2 with $AlH_3{\cdot}NMe_2Et$ and characterized it to show that it is a reaction intermediate in the Ti-catalyzed aluminum nanoparticle synthesis.

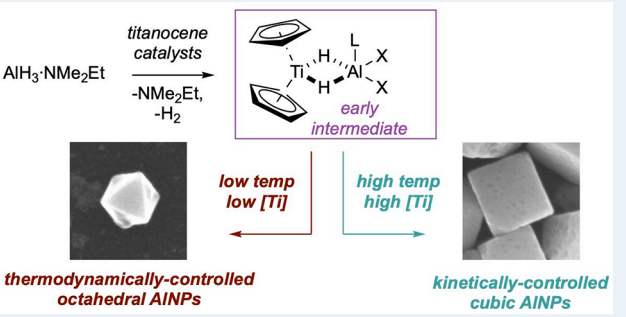

KEYWORDS: *Aluminum nanoparticles, Titanium catalysts, Titanocene, Shape control, Dehydrogenation, Bimetallic complex*

INTRODUCTION

Metal nanoparticles (NPs) have been widely used in many applications such as catalysis and sensing owing to their unique optical properties, in particular, localized surface plasmon resonance (LSPR).[1,2] The size, shape, and the surrounding environment of the nanoparticles influence LSPR, which has prompted extensive research into the controlled synthesis of nanoparticles with specific size and shape characteristics.[3,4] Considerable progress has been achieved in the study of noble-metal-based nanoparticles, such as gold (Au) and platinum (Pt) NPs, by tuning their size and shape and elucidating their formation mechanism.[5−9] However, the demand for cost-effective material has been increasing, and aluminum (Al) is an attractive candidate among metals because Al is the most abundant metal in Earth's crust and can achieve LSPR across the IR, visible, and UV regions.[10] There have been efforts to understand the mechanism(s) of Al nanoparticle (AlNP) formation,[11,12] but there remain significant gaps in our understanding owing to intrinsic difficulties in handling reactive AlNP precursors and because—unlike noble metal NP synthesis—AlNP formation occurs in the presence of catalysts, which are typically Ti-based.

The Halas group has undertaken extensive investigation to gain insight into the role of Ti catalysts in the AlNP synthesis process and to achieve controllable AlNP morphologies.[13−16] The fundamental steps in AlNP synthesis are proposed to include (i) the formation of Ti/Al heterometallic intermediates, (ii) the dehydrogenation of alane (AlH_3, the precursor of Al NPs), and (iii) the subsequent formation of Al−Al bonds. Comprehensive evidence for each of these steps and the overall mechanism remains elusive. It has also been reported that different ligands of the Ti complexes can control the growth and subsequent morphology of the AlNPs.[13,16] Notably, Ti catalysts containing the titanocene moiety (Cp_2Ti−, Cp = cyclopentadienyl) have demonstrated the ability to produce cubic AlNPs. However, further investigations are required to unravel the factors of the catalyst structure and reaction conditions that influence the shape of AlNPs and enable precise modification.

Overall, the mechanisms and controlling factors of Ti-catalyzed alane dehydrocoupling remain poorly understood despite an increased interest in solid aluminum hydride dehydrogenation for hydrogen storage.[17−19] However, there have been significant advances in related dehydrocoupling

Received: October 12, 2024
Revised: November 22, 2024
Accepted: November 22, 2024
Published: December 2, 2024

https://doi.org/10.1021/acscatal.4c06286
ACS Catal. 2024, 14, 18429−18435

reactions such as dehydrocoupling of an amine-borane adduct by titanocene (or zirconacene) catalysts[20−30] and Al^{III} hydride catalysts.[31] In addition, recent studies of dehydrogenation of aluminum dihydride have highlighted the potential of this chemistry.[32,33] These prior studies indicate that understanding, and ultimately control of, alane dehydrocoupling should be possible.

In this study, we present a systematic study of reaction conditions for the optimization of the controlled synthesis of AlNPs, shedding light on how each set of reaction conditions impacts the resulting morphology with a particular focus on how the kinetics of AlNP formation/alane dehydrocoupling impact resultant AlNP morphology. Additionally, we isolated and characterized a bridged Ti−Al heterobimetallic compound, which was demonstrated to be an early reaction intermediate through further reactivity studies.

RESULTS AND DISCUSSION

Prior work from the Halas group on AlNP morphology control focused on $Ti(O^iPr)_4$ and Cp_2Ti derivatives. These studies revealed that $Ti(O^iPr)_4$ yields truncated octahedron AlNPs having both {111} and {100} facets, in alignment with the Wulff theorem for FCC metals, while Cp_2Ti derivatives led to cubic AlNPs with {100} facets.[5]

To start our investigation, we sought to examine how Ti catalyst structure could impact the morphology of AlNPs with a wider range of Ti catalysts under a broad range of temperatures (40−65 °C) and catalyst loadings (0.1 mol % to 1 mol % of [AlH_3·NMe_2Et]). Simple TiX_4-type (X = anionic ligand) catalysts ($Ti(O^iPr)_4$, $TiCl_4$, $Ti(NMe_2)_4$, $TiBn_4$, and $TpTiCl_3$ (Tp = Tris(pyrazolyl)borate)) all produce predominantly truncated octahedra regardless of the ligand with 1 mol % of catalyst loading at 40 °C (Figure 1, Figures S3 and S4). A

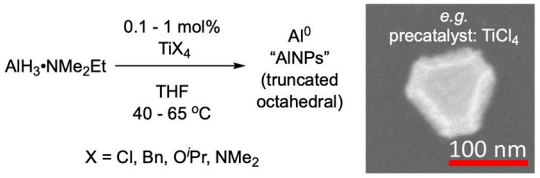

Figure 1. Dehydrocoupling of alane with a simple TiX_4 catalyst leads to truncated octahedral nanocrystals. Right: SEM image of AlNPs synthesized using 1 mol % of $TiCl_4$ at 40 °C.

deeper examination of $Ti(O^iPr)_4$-catalyzed reactions revealed successful truncated octahedral AlNP formation with catalyst loadings ranging from 0.1 mol % to 1 mol % at 40 °C, although at higher temperatures of 50 and 60 °C, the Al NPs became irregularly shaped or fused.

In contrast to the TiX_4-type catalysts, Cp_2Ti-bearing catalysts yielded either cubic or octahedral-shaped Al NPs, depending on reaction conditions (Figure 2, Figure S5). $[Cp_2TiCl]_2$ selectively catalyzes the formation of cubic AlNPs under higher temperature (e.g., 65 °C) and higher catalyst loading conditions (e.g., 0.5 mol %), while under lower temperature (e.g., 40 °C) and lower catalyst loading (e.g., 0.05 mol %) conditions, AlNPs are predominantly octahedral. Under the cubic AlNP reaction conditions, right bipyramid shapes were also produced with the Al nanocubes. Both have {100} facets, but the right bipyramids grow from singly twinned seeds, while the cubes originate from single crystal seeds (Figure S5).[34] The shape control by varying temperature

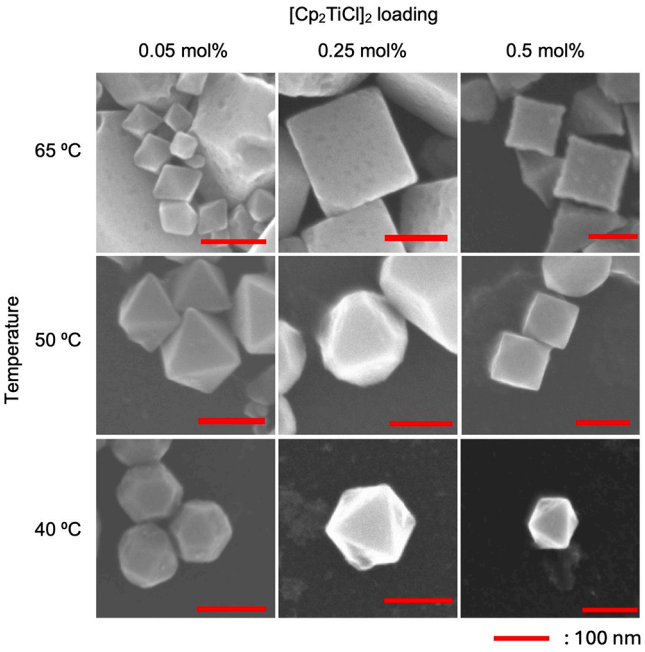

Figure 2. SEM images of shape-controlled AlNP syntheses using $[Cp_2TiCl]_2$ (0.05−0.5 mol %) at 40−65 °C. [AlH_3·NMe_2Et]: 1 mM in THF.

and catalyst loading was not confined to $[Cp_2TiCl]_2$: other precatalysts containing the Cp_2Ti group, including Cp_2TiCl_2, Tebbe's reagent ($Cp_2Ti(\mu\text{-}CH_2)(\mu\text{-}Cl)Al(CH_3)_2$), and Cp_2Ti-(BTMSA) (BTSMA = bis(trimethylsilyl)acetylene) also showed the same effect (Figure 3 and Figures S6 and S7).

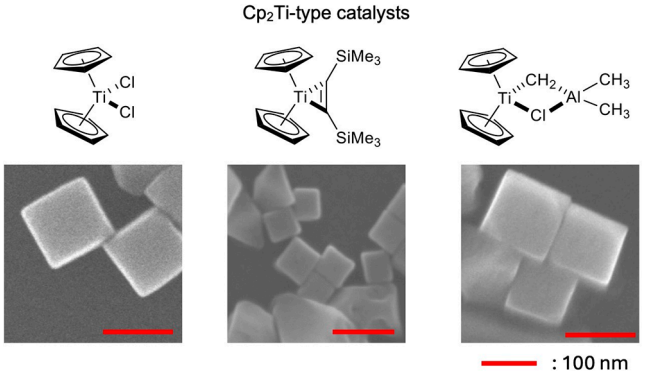

Figure 3. SEM images of cubic AlNPs with other Cp_2Ti-type catalysts (Cp_2TiCl_2, Cp_2Ti(BMTSA), $Cp_2Ti(\mu\text{-}CH_2)(\mu\text{-}Cl)Al(CH_3)_2$, conditions: 1 mol % [Ti], 65 °C, [AlH_3·NMe_2Et]: 1 mM in THF).

These results indicate that the oxidation state of the Ti precatalyst is not correlated to the shape of the AlNPs since the formal oxidation states for the preceding complexes range from Ti(II) to Ti(IV). This is perhaps to be expected, as AlH_3 is a strong reductant that should be able to easily reduce Ti(IV). Interestingly, $CpTiCl_3$, a Ti precatalyst containing only 1 Cp ring, led to octahedral AlNP formation even at 65 °C and under 1 mol % catalyst loading, showing that cubic shape control from the catalyst appears to rigorously require a metallocene fragment (Figure S8).

Given that AlNP shape control could be modulated with titanocene precatalysts under different conditions, we next conducted experiments where the reaction conditions were

https://doi.org/10.1021/acscatal.4c06286
ACS Catal. 2024, 14, 18429−18435

varied *in situ* to study whether (1) shape control was dictated at the seeding stage vs crystal growth phase and (2) one shape could be interconverted into the other.

First, the shape of AlNPs as they grow over time was observed by quenching aliquots of a "cube-controlled" reaction (0.5 mol % of $[Cp_2TiCl]_2$ at 60 °C) every 10 min and monitoring shape by SEM. At early stages (<50 min), the AlNPs were multifaceted, containing both {100} and {111} facets (Figure S10). The {100} facet proportion increased as the NPs grew larger over time, showing clear nanocubes at 70 min of the reaction. At 90 min, most of the NPs were cubic, with some elongated and fused NPs. The findings indicate that the clear cubic shape is determined after nanoseed or nanocluster formation.

Next, an "octahedral-controlled" reaction (0.05 mol % of $[Cp_2TiCl]_2$ at 50 °C) was dosed with additional 0.45 mol % $[Cp_2TiCl]_2$, resulting in total 0.5 mol % Ti, at different time points to probe if octahedrally shaped seeds could be converted to cubic AlNPs. Every attempt yielded cubic AlNPs (Figure 4a, Figure S11), which further demonstrates

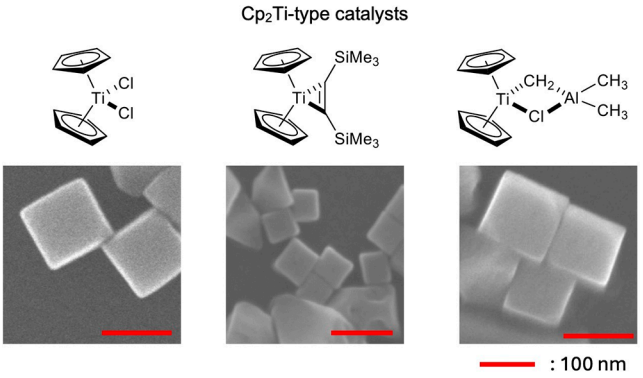

Figure 4. SEM images of AlNPs after changing reaction conditions *in situ*. (a) Increase in catalyst concentration. (b) Change in temperature. $NR_3 = NMe_2Et$.

that shape is determined in the middle or late phase of AlNP synthesis, consistent with the quenching experiments described above. The size of Al nanocubes formed when the stock solution was added after 20 min was larger than that of cubes formed after the stock solution was added after 50 min because the shorter seeding time likely leads to fewer seeding events, and the seeds can then grow larger owing to the relatively larger amount of Al for fewer seeds.

Finally, *in situ* temperature changes were examined. Raising the reaction temperature from 40 °C to 65 °C in the middle of the reaction (after 1.5 or 3 h) produced more {100} facets than reactions held at 40 °C, leading to elongated rodlike crystals with {100} sides (Figure 4b). Here, the increase in temperature likely facilitates faster Al reduction, leading to the formation of a structure with more {100} facets on the preexisting Al nanoseeds. On the other hand, decreasing the temperature from 65 °C to 40 °C after 50 min yielded inhomogeneous shapes, probably because reactive Al nanoclusters could not grow larger due to an insufficient amount of reduced Al, causing them to fuse together.

The above experiments indicate that the rate of Al reduction and deposition under different reaction conditions (temperature or catalyst concentration) during AlNP growth is a key factor in determining their shape. Thus, we next conducted kinetic studies of $AlH_3{\cdot}NMe_2Et$ dehydrogenation using Cp_2TiCl_2 as the catalyst across different catalyst loadings (Figure 5a) and temperature regimes (Figure 5b). In all cases,

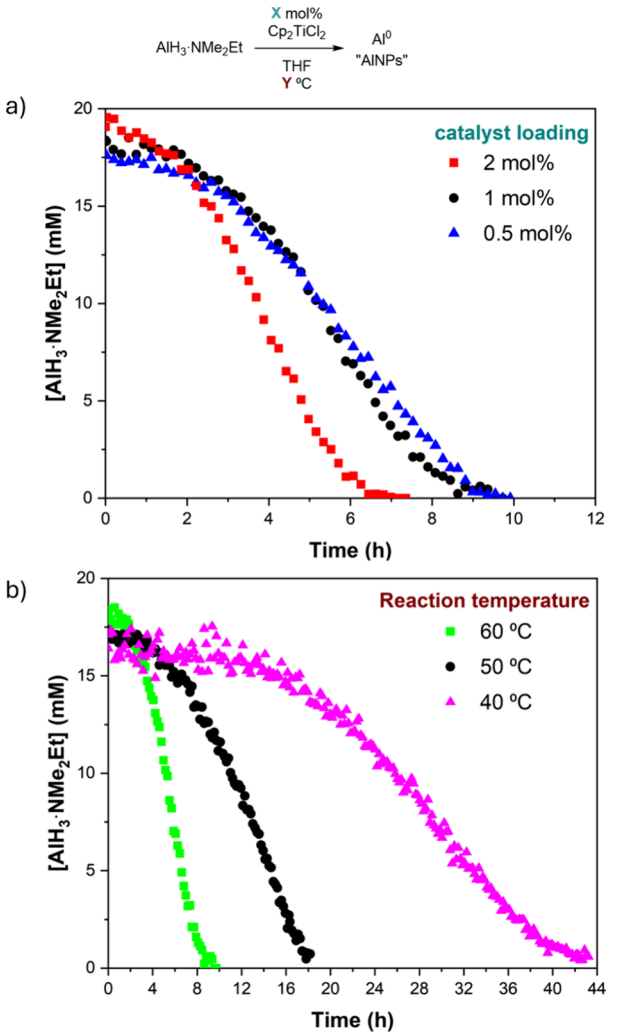

Figure 5. Kinetic trace of $AlH_3{\cdot}NMe_2Et$ dehydrogenation in THF-d_8 (a) with different catalyst loadings of Cp_2TiCl_2 at 60 °C and (b) different reaction temperatures with 1 mol % of Cp_2TiCl_2.

the consumption of $AlH_3{\cdot}NMe_2Et$ shares a common shape characterized by a slower induction period, followed by a faster decay. These features indicate that $AlH_3{\cdot}NMe_2Et$ reacts with the Ti complex, likely predominantly forming Ti/Al clusters during the induction period. Then, after a critical seeding period, $AlH_3{\cdot}NMe_2Et$ undergoes rapid catalytic dehydrogenation−reduction and deposition onto growing seeds. SEM analysis and UV/vis spectroscopy were also used to monitor the reaction behavior during the induction period and the faster decay phase (Figures S13 and S14). The results showed that a small number of immature AlNPs formed during the induction period, while the majority were rapidly formed after the faster decay, consistent with the NMR analysis. At higher catalyst concentrations or temperatures, the slope of the catalytic reaction period is steep, indicating that Al reduction is rapid and Al nanocubes are selectively formed, suggesting that the cubic shape is kinetically controlled.

To test the hypothesis that cubic AlNP formation was kinetically controlled, we next explored catalytic AlNP formation under a purge of H_2 gas. As H_2 is a byproduct of

https://doi.org/10.1021/acscatal.4c06286
ACS Catal. 2024, 14, 18429−18435

dehydrogenation, introduction of excess H_2 into the headspace could perturb the equilibrium of dehydrogenation and result in overall slower AlNP growth. As hypothesized, the reaction of $AlH_3{\cdot}NMe_2Et$ with $[Cp_2TiCl]_2$ at high concentration and temperature under a purge of H_2 results in truncated octahedral AlNPs (Figure S12). Because the equilibrium of alane dehydrogenation is perturbed by increasing $[H_2]$, the rate of Al_0 formation and deposition decreases, while the rate of Al^0 diffusion remains constant, since the reaction temperature is unchanged. Al^0 can then be relocated to thermodynamically more stable sites, yielding octahedra under thermodynamic rather than kinetic control.

Of particular interest is how reduced Al clusters initially form during the catalytic induction period prior to AlNP growth. Here, we are undertaking studies to isolate and characterize early reaction intermediates, including Ti−Al heterobimetallic complexes. Reaction of Cp_2TiCl_2 with 1 equiv of $AlH_3{\cdot}NMe_2Et$ in THF for an hour yielded a purple solution containing Ti−Al bimetallic complex **1** ($Cp_2Ti(\mu_2\text{-}H_2)\text{-}AlCl_2(THF)$). Repeated *in vacuo* drying of the reaction mixture followed by redissolution into THF was critical to remove excess NMe_2Et from the reaction, which then enabled the crystallization of **1** from a pentane/*p*-xylene mixture at −35 °C. The solid state structure of **1** is reported in Figure 6. A similar compound coordinated by Et_2O instead of THF was previously synthesized through the reaction of $AlH_3{\cdot}Et_2O$ with Cp_2TiCl_2.[35] In addition to **1**, several Ti/Al bimetallic or multimetal complexes sharing the same motif, [Ti-μ_2H_2-Al], have been reported.[36−40] All of these complexes feature a Cp (or Cp*) ligand on Ti, suggesting that the Cp ligand provides the stability necessary for isolation.

From a simple electron-counting analysis, the limiting electronic structures of **1** could be either Ti^{III}/Al^{III} or Ti^{IV}/Al^{II}, indicating a net reduction of the system en route to full reduction of alane. **1** contains two bridging hydrides, with Ti−H average bond lengths of 1.797 Å (1.757, 1.821, 1.813, 1.797 Å of two complexes, respectively, in the unit cell), which are slightly longer than the average Ti^{IV}−H bond length (1.781 Å) but shorter than Ti^{III}−H (1.865 Å).[41] Since **1** is paramagnetic, it was characterized by EPR spectroscopy to better understand the electronic structure (Figure 6c). **1** has a *g* value of 1.987, with hyperfine splitting parameters A_{Ti} = 15, A_{Al} = 29.5, A_H = 9.7, and A_{Cl} = 1.9. The hyperfine couplings of atoms in the [Ti-μ_2H_2-Al] scaffold indicates that the best description of **1** is a delocalized radical shared between the metal centers rather than a formally Ti^{III}/Al^{III} or Ti^{IV}/Al^{II} complex. Excitingly, **1** acts as a precatalyst for $AlH_3{\cdot}NMe_2Et$ dehydrogenation, yielding AlNPs identical to those formed from Cp_2TiCl_2 with similar kinetic behavior, indicating that **1** is an early intermediate en route to productive catalysis (Figure 7). Catalysis with **1** still reveals an induction period, indicating that there are still more key intermediates to be investigated in the future.

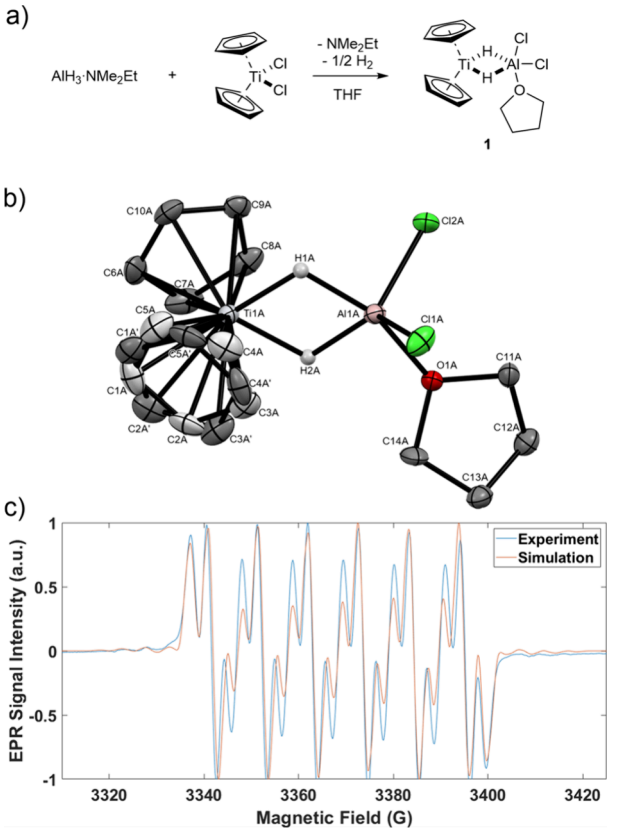

Figure 6. Reaction intermediate **1** isolation and characteristics. (a) Reaction scheme of the synthesis of **1**. (b) Molecular structures of **1**. One complex in the unit cell (Z = 2) is shown. *p*-Xylene cosolvent and hydrogen atoms except bridging hydrides are omitted for clarity. Light gray ellipsoids are disordered Cp. Ellipsoids are drawn at the 50% probability level. Selected bond distances (Å): Ti1A−H1A 1.757, Ti1A−H2A 1.821, Al1A−H1A 1.730, and Al1A−H2A 1.678. (c) Experimental and simulated EPR spectra of **1**.

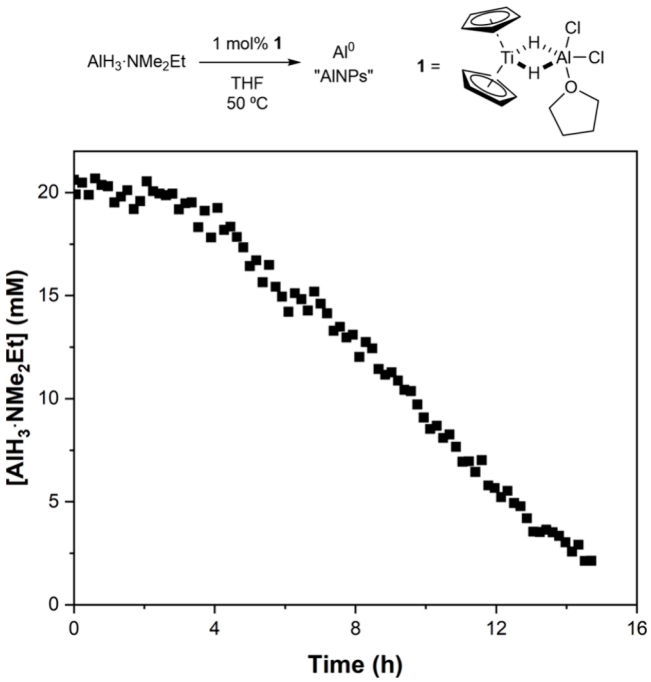

Figure 7. Kinetic trace of $AlH_3{\cdot}NMe_2Et$ dehydrogenation catalyzed by **1**. Conditions: 20 mM [Al], 50 °C, and 0.2 mM **1** in THF.

Based on the above studies into the kinetics of AlNP formation under various conditions, we can propose a more detailed reaction mechanism for shape-controlled AlNP synthesis (Figure 8). First, Ti precatalysts form a [Ti-μ_2H_2-Al] intermediate with one equivalent of alane, which then likely proceeds to make larger Ti/Al multimetal clusters via additional dehydrocoupling reactions with alane. The reaction

https://doi.org/10.1021/acscatal.4c06286
ACS Catal. 2024, 14, 18429−18435

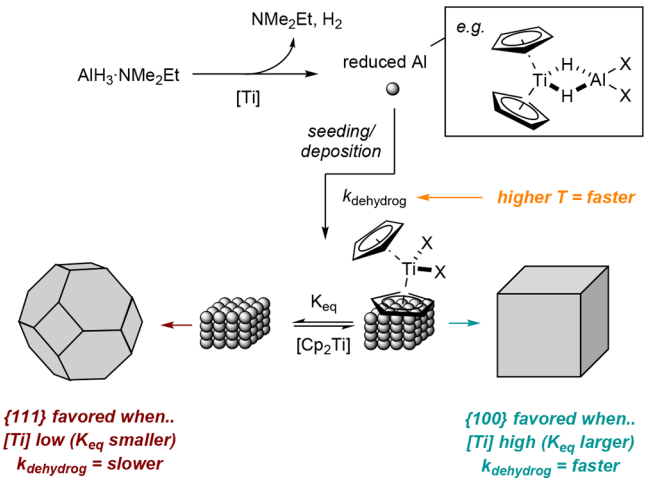

Figure 8. Proposed mechanism for AlNP shape control catalyzed by Cp_2Ti-derived catalysts.

eventually reduces Al^{3+} to Al adatoms growing into "nano-seeds". With titanocene catalysts, competing kinetic and thermodynamic regimes dictate the AlNP shape. Prior work from the Halas group indicates that Cp rings can bind to the Al NP surface through π-electron interaction of the arene,[13] affecting its shape by modulating surface energy.[5] At high catalyst concentration and high temperature, the rate of nanoseed formation (dehydrogenation and deposition) is high, along with significant catalyst-bound surface coverage (see Supporting Information), resulting in kinetic deposition onto the {111} facet, leading to cubic AlNPs. In contrast at low catalyst concentration or temperature, dehydrogenation and deposition are slower and there are fewer catalyst-bound AlNPs under the equilibrium conditions, leading to the formation of thermodynamically controlled octahedral shape. Thus, counterintuitively, less-stable cubic {100} AlNPs are formed at higher temperature, while more stable octahedral {111} AlNPs are formed at lower temperature.[5] In contrast, TiX_4-type catalysts do not have capping effects through arene–surface interaction, leading solely to octahedral shapes across all concentration and temperature regimes. However, simple capping effects are not solely responsible for cubic Al NP formation: for example, the potentially capping precatalyst $CpTiCl_3$ does not produce cubic Al NPs, even at high precatalyst stoichiometries where there are sufficient Cp groups to fully cap all Al surfaces (Figure S9). This highlights the critical role of the overall catalyst structure in addition to capping effects.

CONCLUSION

In conclusion, we have systematically studied how the shape of AlNPs is controlled by using Cp_2Ti-type precatalysts. At high temperature and catalyst concentration, the cubic shape predominates, but in low temperature and catalyst concentration, a truncated octahedral shape results. These two shapes can be described as the kinetic- or thermodynamic-controlled shape, respectively. This work provides further evidence that the mechanism for cubic shape control is likely a function of Cp surface binding equilibria,[11,15] although the morphology of seeds[13] remains in question. In addition, the reaction of Cp_2TiCl_2 and alane yielded the Ti/Al heterobimetallic complex (**1**), which was characterized by XRD and EPR. Complex **1** is an early intermediate in the Al NP synthesis and aligns with prior *in situ* studies,[15] although reactions catalyzed by **1** still have an induction period, meaning that further transformations must take place before rapid Al deposition.

ASSOCIATED CONTENT

Supporting Information

The Supporting Information is available free of charge at https://pubs.acs.org/doi/10.1021/acscatal.4c06286.

Full experimental section (synthesis, SEM images, kinetic study, and simple calculation of Cp coverage on AlNP surface) (PDF)

Crystallographic details (CIF)

AUTHOR INFORMATION

Corresponding Author

Ian A. Tonks − *Department of Chemistry, University of Minnesota−Twin Cities, Minneapolis, Minnesota 55455, United States;* orcid.org/0000-0001-8451-8875; Email: itonks@umn.edu

Authors

Jaekwan Kim − *Department of Chemistry, University of Minnesota−Twin Cities, Minneapolis, Minnesota 55455, United States*

Christian R. Jacobson − *Department of Chemistry and Laboratory for Nanophotonics, Rice University, Houston, Texas 77005, United States;* orcid.org/0000-0002-9578-8763

Naomi J. Halas − *Department of Chemistry and Laboratory for Nanophotonics, Rice University, Houston, Texas 77005, United States; Department of Physics and Astronomy, Department of Electrical and Computer Engineering, Rice University, Houston, Texas 77005, United States;* orcid.org/0000-0002-8461-8494

Complete contact information is available at: https://pubs.acs.org/10.1021/acscatal.4c06286

Author Contributions

N.J.H. and I.A.T. conceived of and directed the research. J.K. planned and executed the research and data analysis. C.R.J. conducted initial experiments and assisted in data analysis. All authors contributed to the writing and revision of the manuscript.

Notes

The authors declare no competing financial interest.

ACKNOWLEDGMENTS

Financial support was provided by the National Science Foundation (2154998) and the University of Minnesota Department of Chemistry (4th year Excellence Fellowship to J.K.). Instrumentation for the University of Minnesota Chemistry NMR facility was supported from a grant through the National Institutes of Health (S10OD011952). Funding for NMR instrumentation at the Minnesota NMR Center was provided by the Office of the Vice President for Research, the Medical School, the College of Biological Science, NIH, NSF, and the Minnesota Medical Foundation. X-ray diffraction experiments were performed with a diffractometer purchased through a grant from NSF/MRI (1229400) and the University of Minnesota. Dr. Victor G. Young Jr. is acknowledged for helping to solve the crystal structure. Parts of this work were carried out in the Characterization Facility, University of

Minnesota, which receives partial support from the NSF through the MRSEC (Award Number DMR-2011401) and the NNCI (Award Number ECCS-2025124) programs.

REFERENCES

(1) Chan, G. H.; Zhao, J.; Schatz, G. C.; Duyne, R. P. V. Localized Surface Plasmon Resonance Spectroscopy of Triangular Aluminum Nanoparticles. *J. Phys. Chem. C* **2008**, *112*, 13958−13963.
(2) Knight, M. W.; King, N. S.; Liu, L.; Everitt, H. O.; Nordlander, P.; Halas, N. J. Aluminum for Plasmonics. *ACS Nano* **2014**, *8*, 834−840.
(3) Cuenya, B. R. Synthesis and Catalytic Properties of Metal Nanoparticles: Size, Shape, Support, Composition, and Oxidation State Effects. *Thin Solid Films* **2010**, *518*, 3127−3150.
(4) An, K.; Somorjai, G. A. Size and Shape Control of Metal Nanoparticles for Reaction Selectivity in Catalysis. *ChemCatChem.* **2012**, *4*, 1512−1524.
(5) Xia, Y.; Xia, X.; Peng, H. C. Shape-Controlled Synthesis of Colloidal Metal Nanocrystals: Thermodynamic versus Kinetic Products. *J. Am. Chem. Soc.* **2015**, *137*, 7947−7966.
(6) Shi, Y.; Lyu, Z.; Zhao, M.; Chen, R.; Nguyen, Q. N.; Xia, Y. Noble-Metal Nanocrystals with Controlled Shapes for Catalytic and Electrocatalytic Applications. *Chem. Rev.* **2021**, *121*, 649−735.
(7) Xie, S.; Choi, S. Il; Xia, X.; Xia, Y. Catalysis on Faceted Noble-Metal Nanocrystals: Both Shape and Size Matter. *Current Opinion in Chemical Engineering* **2013**, *2*, 142−150.
(8) Pal, J.; Pal, T. Faceted Metal and Metal Oxide Nanoparticles: Design, Fabrication and Catalysis. *Nanoscale* **2015**, *7*, 14159−14190.
(9) Zhang, Z.; Wang, Z.; Zhang, H.; Wang, C.; Yin, Y.; Jin, M. Monitoring the Shape Evolution of Pd Nanocubes to Octahedra by PdS Frame Markers. *Nanoscale* **2014**, *6*, 3518−3521.
(10) Yang, S.; Lu, S.; Li, Y.; Yu, H.; He, L.; Sun, T.; Yang, B.; Liu, K. Poly(Ethylene Oxide) Mediated Synthesis of Sub-100-Nm Aluminum Nanocrystals for Deep Ultraviolet Plasmonic Nanomaterials. *CCS Chemistry* **2020**, *2*, 516−526.
(11) Clark, B. D.; Desantis, C. J.; Wu, G.; Renard, D.; McClain, M. J.; Bursi, L.; Tsai, A. L.; Nordlander, P.; Halas, N. J. Ligand-Dependent Colloidal Stability Controls the Growth of Aluminum Nanocrystals. *J. Am. Chem. Soc.* **2019**, *141*, 1716−1724.
(12) Jacobson, C. R.; Solti, D.; Renard, D.; Yuan, L.; Lou, M.; Halas, N. J. Shining Light on Aluminum Nanoparticle Synthesis. *Acc. Chem. Res.* **2020**, *53*, 2020−2030.
(13) Dhindsa, P.; Solti, D.; Jacobson, C. R.; Kuriakose, A.; Naidu, G. N.; Bayles, A.; Yuan, Y.; Nordlander, P.; Halas, N. J. Facet Tunability of Aluminum Nanocrystals. *Nano Lett.* **2022**, *22*, 10088−10094.
(14) Lu, S.; Yu, H.; Gottheim, S.; Gao, H.; Desantis, C. J.; Clark, B. D.; Yang, J.; Jacobson, C. R.; Lu, Z.; Nordlander, P.; Halas, N. J.; Liu, K. Polymer-Directed Growth of Plasmonic Aluminum Nanocrystals. *J. Am. Chem. Soc.* **2018**, *140*, 15412−15418.
(15) Clark, B. D.; Jacobson, C. R.; Lou, M.; Renard, D.; Wu, G.; Bursi, L.; Ali, A. S.; Swearer, D. F.; Tsai, A. L.; Nordlander, P.; Halas, N. J. Aluminum Nanocubes Have Sharp Corners. *ACS Nano* **2019**, *13*, 9682−9691.
(16) Jacobson, C. R.; Wu, G.; Alemany, L. B.; Naidu, G. N.; Lou, M.; Yuan, Y.; Bayles, A.; Clark, B. D.; Cheng, Y.; Ali, A.; Tsai, A. L.; Tonks, I. A.; Nordlander, P.; Halas, N. J. A Dual Catalyst Strategy for Controlling Aluminum Nanocrystal Growth. *Nano Lett.* **2022**, *22*, 5570−5574.
(17) Ikeda, K.; Muto, S.; Tatsumi, K.; Menjo, M.; Kato, S.; Bielmann, M.; Züttel, A.; Jensen, C. M.; Orimo, S. Dehydriding Reaction of AlH_3: In Situ Microscopic Observations Combined with Thermal and Surface Analyses. *Nanotechnology* **2009**, *20*, 204004.
(18) Chen, S.; Tang, Y.; Yu, H.; Bao, L.; Zhang, W.; DeLuca, L. T.; Shen, R.; Ye, Y. The Rapid H_2 Release from AlH_3 Dehydrogenation Forming Porous Layer in AlH_3/Hydroxyl-Terminated Polybutadiene (HTPB) Fuels during Combustion. *J. Hazard. Mater.* **2019**, *371*, 53−61.
(19) Jiang, W.; Wang, H.; Zhu, M. AlH_3 as a Hydrogen Storage Material: Recent Advances, Prospects and Challenges. *Rare Met.* **2021**, *40*, 3337−3356.
(20) Clark, T. J.; Russell, C. A.; Manners, I. Homogeneous, Titanocene-Catalyzed Dehydrocoupling of Amine-Borane Adducts. *J. Am. Chem. Soc.* **2006**, *128*, 9582−9583.
(21) Pun, D.; Lobkovsky, E.; Chirik, P. J. Amineborane Dehydrogenation Promoted by Isolable Zirconium Sandwich, Titanium Sandwich and N_2 Complexes. *Chem. Commun.* **2007**, *31*, 3297−3299.
(22) Sloan, M. E.; Staubitz, A.; Clark, T. J.; Russell, C. A.; Lloyd-Jones, G. C.; Manners, I. Homogeneous Catalytic Dehydrocoupling/Dehydrogenation of Amine-Borane Adducts by Early Transition Metal, Group 4 Metallocene Complexes. *J. Am. Chem. Soc.* **2010**, *132*, 3831−3841.
(23) Chapman, A. M.; Haddow, M. F.; Wass, D. F. Frustrated Lewis Pairs beyond the Main Group: Cationic Zirconocene- Phosphinoaryloxide Complexes and Their Application in Catalytic Dehydrogenation of Amine Boranes. *J. Am. Chem. Soc.* **2011**, *133*, 8826−8829.
(24) Beweries, T.; Thomas, J.; Klahn, M.; Schulz, A.; Heller, D.; Rosenthal, U. Catalytic and Kinetic Studies of the Dehydrogenation of Dimethylamine Borane with an IPr Substituted Titanocene Catalyst. *ChemCatChem.* **2011**, *3*, 1865−1868.
(25) Nomura, K.; Liu, J. Half-Titanocenes for Precise Olefin Polymerisation: Effects of Ligand Substituents and Some Mechanistic Aspects. *Dalton Trans.* **2011**, *40*, 7666−7682.
(26) Chapman, A. M.; Wass, D. F. Cationic Ti(IV) and Neutral Ti(III) Titanocene-Phosphinoaryloxide Frustrated Lewis Pairs: Hydrogen Activation and Catalytic Amine-Borane Dehydrogenation. *Dalton Trans.* **2012**, *41*, 9067−9072.
(27) Helten, H.; Dutta, B.; Vance, J. R.; Sloan, M. E.; Haddow, M. F.; Sproules, S.; Collison, D.; Whittell, G. R.; Lloyd Jones, G. C.; Manners, I. Paramagnetic Titanium(III) and Zirconium(III) Metallocene Complexes as Precatalysts for the Dehydrocoupling/Dehydrogenation of Amine-Boranes. *Angew. Chem., Int. Ed.* **2013**, *52*, 437−440.
(28) Metters, O. J.; Flynn, S. R.; Dowds, C. K.; Sparkes, H. A.; Manners, I.; Wass, D. F. Catalytic Dehydrocoupling of Amine-Boranes Using Cationic Zirconium(IV)-Phosphine Frustrated Lewis Pairs. *ACS Catal.* **2016**, *6*, 6601−6611.
(29) Lapierre, E. A.; Patrick, B. O.; Manners, I. Trivalent Titanocene Alkyls and Hydrides as Well-Defined, Highly Active, and Broad Scope Precatalysts for Dehydropolymerization of Amine-Boranes. *J. Am. Chem. Soc.* **2019**, *141*, 20009−20015.
(30) Lindenau, K.; Jannsen, N.; Rippke, M.; Al Hamwi, H.; Selle, C.; Drexler, H.-J.; Spannenberg, A.; Sawall, M.; Neymeyr, K.; Heller, D.; Reiß, F.; Beweries, T. Mechanistic Insights into Dehydrocoupling of Amine Boranes Using Dinuclear Zirconocene Complexes. *Catal. Sci. Technol.* **2021**, *11*, 4034−4050.
(31) Weetman, C.; Ito, N.; Unno, M.; Hanusch, F.; Inoue, S. NHI- and NHC-Supported Al(III) Hydrides for Amine-Borane Dehydrocoupling Catalysis. *Inorganics* **2019**, *7*, 92.
(32) Nako, A. E.; Gates, S. J.; Schädel, N.; White, A. J. P.; Crimmin, M. R. Yttrium-Catalysed Dehydrocoupling of Alanes with Amines. *Chem. Commun.* **2014**, *50*, 9536−9538.
(33) Hooper, T. N.; Lau, S.; Chen, W.; Brown, R. K.; Garçon, M.; Luong, K.; Barrow, N. S.; Tatton, A. S.; Sackman, G. A.; Richardson, C.; White, A. J. P.; Cooper, R. I.; Edwards, A. J.; Casely, I. J.; Crimmin, M. R. The Partial Dehydrogenation of Aluminium Dihydrides. *Chem. Sci.* **2019**, *10*, 8083−8093.
(34) Skrabalak, S. E.; Xia, Y. Pushing Nanocrystal Synthesis toward Nanomanufacturing. *ACS Nano* **2009**, *3*, 10−15.
(35) Lobkovskii, E. B.; Soloveichik, G. L.; Bulychev, B. M.; Gerr, R. G.; Struchkov, Y. T. Structural chemistry of titanium and aluminium bimetallic hydride complexes II. Crystal and molecular structure of $(\eta^5\text{-}C_5H_5)_2Ti(\mu\text{-}H)_2AlCl_2{\cdot}O(C_2H_5)_2$. *J. Organomet. Chem.* **1984**, *270*, 45−51.
(36) Lobkovskii, E. B.; Soloveichik, G. L.; Sisov, A. I.; Bulychev, B. M.; Gusev, A. I.; Kirillova, N. I. Structural Chemistry of Bimetallic Hydride Complexes of Titanium and Aluminium I. Crystal and

Molecular Structure of $[(\eta^5\text{-}C_5H_5)_2Ti(\mu\text{-}H)_2AlH_2]_2(CH_3)_2NCH_2CH_2N(CH_3)_2C_6H_6$. *J. Organomet. Chem.* **1984**, *265*, 167−173.

(37) Lobkovskii, E. B.; Soloveichik, G. L.; Sizov, A. I.; Bulychev, B. M. Structural Chemistry of Titanium and Aluminium Bimetallic Hydride Complexes III. Synthesis, Molecular Structure and Catalytic Properties of $[(\eta^5\text{-}C_5H_5)_2Ti(\mu_2\text{-}H)_2Al(\mu_2\text{-}H)(\eta^5{:}\eta^1\text{-}C_5H_4)Ti(\eta^5\text{-}C_5H_5)(\mu_2\text{-}H)]_2{\cdot}C_6H_5CH_3$. *J. Organomet. Chem.* **1985**, *280*, 53−66.

(38) Bel'sky, V. K.; Sizov, A. I.; Bulychev, B. M.; Soloveichik, G. L. Structural Chemistry of Titanium and Aluminium Bimetallic Hydride Complexes IV. Molecular Structures and Catalytic Properties of $\{[\eta^5\text{-}C_5(CH_3)_5]_2Ti(\mu_2\text{-}H)_2Al(H)(\mu_2\text{-}H)\}_2$ and $[\eta^5\text{-}C_5(CH_3)_5]_2Ti(\mu_2\text{-}H)_2Al(H)(\mu_2\text{-}H)_2Ti[\eta^5\text{-}C_5(CH_3)_5]_2$. *J. Organomet. Chem.* **1985**, *280*, 67−80.

(39) Lobkovskii, E. B.; Sizov, A. I.; Bulychev, B. M.; Sokolova, I. V.; Soloveichik, G. L. Structural Chemistry of Titanium and Aluminium Bimetallic Hydride Complexes V. Crystal and Molecular Structure of Octonuclear $\{[(\eta^5\text{-}C_5Me_5)(\eta^5\text{-}C_5Me_3CH_2]Ti(\mu_2\text{-}H)_2Al]_2\text{-}\ \mu_3\text{-}O\}_2{\cdot}2C_6H_6$. *J. Organomet. Chem.* **1987**, *319*, 69−75.

(40) Sizov, A. I.; Molodnitskaya, V.; Bulychev, B. M.; Bel'skii, V. K.; Soloveichii, G. L. Structural Chemistry of Titanium and Aluminium Bimetallic Hydride Complexes VII. Exchange Reactions in the Coordination Sphere of Aluminium Atom. Crystal and Molecular Structure of $[(\eta^5\text{-}C_5H_5)_2Ti(\mu_2\text{-}H)_2]_2Al(\eta^2\text{-}H_2BH_2)$. *J. Organomet. Chem.* **1988**, *344*, 185−193.

(41) Bruno, I. J.; Cole, J. C.; Edgington, P. R.; Kessler, M.; Macrae, C. F.; McCabe, P.; Pearson, J.; Taylor, R. New software for searching the Cambridge Structural Database and visualizing crystal structures. *Acta Crystallogr.* **2002**, *B58*, 389−397.

https://doi.org/10.1021/acscatal.4c06286
ACS Catal. 2024, 14, 18429−18435